

Fatigue behaviour of root crack in stiffener-to-deck plate weld at crossbeam of orthotropic bridge decks

Wu, Weijian; Veljkovic, Milan; Kolstein, Henk; Pijpers, Richard; Maljaars, Johan

DOI

[10.1016/j.engstruct.2024.117710](https://doi.org/10.1016/j.engstruct.2024.117710)

Publication date

2024

Document Version

Final published version

Published in

Engineering Structures

Citation (APA)

Wu, W., Veljkovic, M., Kolstein, H., Pijpers, R., & Maljaars, J. (2024). Fatigue behaviour of root crack in stiffener-to-deck plate weld at crossbeam of orthotropic bridge decks. *Engineering Structures*, 306, Article 117710. <https://doi.org/10.1016/j.engstruct.2024.117710>

Important note

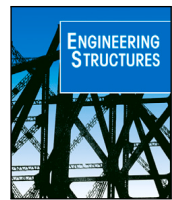
To cite this publication, please use the final published version (if applicable).
Please check the document version above.

Copyright

Other than for strictly personal use, it is not permitted to download, forward or distribute the text or part of it, without the consent of the author(s) and/or copyright holder(s), unless the work is under an open content license such as Creative Commons.

Takedown policy

Please contact us and provide details if you believe this document breaches copyrights.
We will remove access to the work immediately and investigate your claim.



Fatigue behaviour of root crack in stiffener-to-deck plate weld at crossbeam of orthotropic bridge decks

Weijian Wu^{a,*}, Milan Veljkovic^a, Henk Kolstein^a, Richard Pijpers^b, Johan Maljaars^{b,c}

^a Delft University of Technology, Mekelweg 5, Delft, The Netherlands

^b TNO, Molengraaffsingel 8, Delft, The Netherlands

^c Eindhoven University of Technology, Blauwe Zaal 1, Eindhoven, The Netherlands

ARTICLE INFO

Keywords:

Orthotropic bridge deck
Stiffener-to-deck plate weld at crossbeam
Fatigue resistance
Hot spot stress
Crack arrest

ABSTRACT

Steel Orthotropic Bridge Decks (OBDs) are widely used in long-span and movable bridges. Fatigue resistance analysis plays an important role in the design or assessment of OBDs. One possible fatigue failure is the crack initiating from the weld root of stiffener-to-deck plate connections at crossbeams. A full-scale experimental investigation in this study using a 20 mm thick deck plate with a dimension of 9.4 m × 5.1 m, including three crossbeams, represents the modern designed OBDs. The experiments show an arrest of crack propagation with a final crack depth of approximately 75% of the deck plate thickness. On the contrary, through thickness cracks develop in deck plates of 10 or 12 mm. Hot spot stress based fatigue detail categories (DC) using various failure criteria derived from the tests. Analysis with the effective notch stress shows that the DC has low sensitivity to the amount of weld penetration. The results of analyses with the eXtended Finite Element Method (XFEM), employed to analyse the fatigue crack propagation path and crack arrest, are in line with the experimental study.

1. Introduction

Steel Orthotropic Bridge Decks (OBDs) are commonly used for long-span and movable bridges. An OBD consists of a deck plate, stiffened by open or closed longitudinal stiffeners and transverse crossbeams. Characteristics like low self-weight, and fast construction make it attractive for new bridge designs and existing bridge deck replacements [1–4]. In the service life, fatigue cracks have been found in OBDs since the early 1970s [2,5,6]. Fig. 1 shows a representative OBD with the potential crack locations in the stiffener-to-deck plate welded connections. This connection is subjected to high stresses caused by local wheel loading of crossing lorries. Fatigue cracks may occur from the weld toe (types C1a and C2a) or the weld root (types C1b, C1c, and C2b) of the connection and propagate into the deck plate (types C1a, C1b, and C1c) or the stiffener (types C2a and C2b). Root cracks normally have lower fatigue resistances than toe cracks [7]. Root cracks may initiate in span (type C1b) or at the crossbeam intersection (type C1c). This paper studies the latter type, C1c, which accounts for a large proportion of fatigue cracks inspected [8–10]. Back surface breaking cracks (through thickness cracks) were observed in both the laboratory tests and in-site inspections [1,2,9,11,12]. The studies demonstrate that

C1c has a relatively long crack propagation period due to the stress redundancy [9,12], which is confirmed by fracture mechanics calculations [13,14]. The European standard (pr)EN1993-1-9 [15,16] gives the fatigue resistance of many weld details. The resistance is expressed in terms of Detail Category (DC), which is the fatigue resistance in MPa at $2 \cdot 10^6$ cycles with a 95% exceedance probability. Neither the first nor second generation of EN1993-1-9 provides a fatigue resistance for detail C1c. The nominal stress method is unsuitable for detail C1c because of the local stress concentration. (Structural) hot spot stress, alternatively, contains the bending and membrane stress of the plate which is more suitable for this detail [7,17,18]. A hot spot stress DC of 125 is proposed in [1] based on conservative treatment of the test data in [1,2]. The AASHTO specifications [19,20] gives Category C (equivalent to DC 90), the lowest DC for hot spot stress, for detail C1c. Recent research shows that the fatigue resistance of detail C1c is higher than the recommended values, amongst others attributed to the generation of compressive stress under wheel loading at the crack initiation point.

With the increase in traffic volume, a need is identified to construct a new type of OBD with a better fatigue performance. One

* Corresponding author.

E-mail address: w.wu-1@tudelft.nl (W. Wu).

<https://doi.org/10.1016/j.engstruct.2024.117710>

Received 27 October 2023; Received in revised form 9 January 2024; Accepted 18 February 2024

Available online 12 March 2024

0141-0296/© 2024 The Author(s). Published by Elsevier Ltd. This is an open access article under the CC BY license (<http://creativecommons.org/licenses/by/4.0/>).

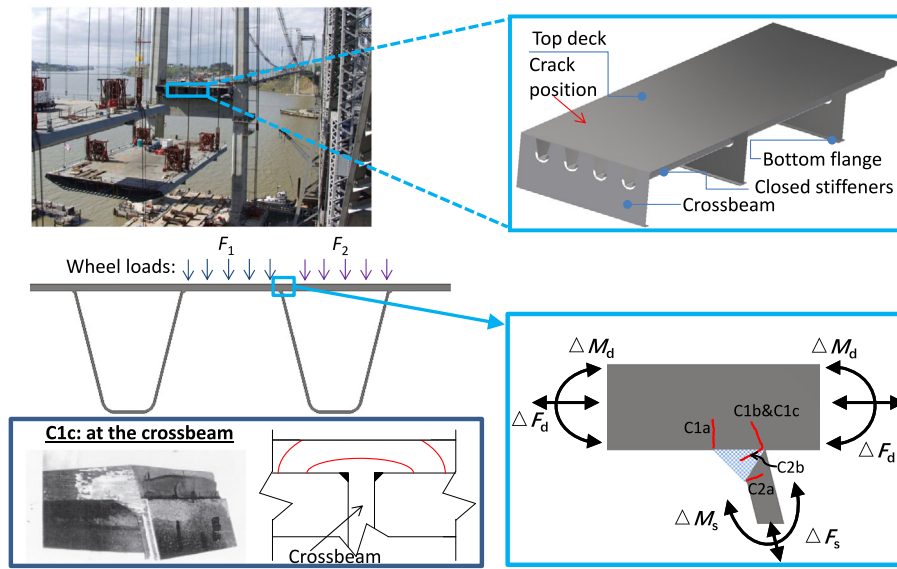


Fig. 1. Construction photo of an OBD and illustrations of stiffener-to-deck cracks.
Source: Photo from [1,20].

easy and effective solution is to increase the deck plate thickness. Maljaars et al. [21] recommend a deck plate thickness ranging from 17 mm to 22 mm for “Cat. 1” type road bridges (with the heaviest traffic flow) with a target service life of 100 years using the fatigue load measured with weigh in motion systems in the Netherlands based on a fracture mechanics assessment. Deck plates ranging from 16 mm to 19 mm are commonly seen in modern OBDs [20,22,23]. However, the recommended DC for detail C1c with these thick deck plates is not available. The authors, therefore, have carried out fatigue experiments using a full-scale OBD specimen with a 20 mm thick deck plate. The specimen contains eight trapezoid shape closed stiffeners that are tested individually. The cracks are inspected using Time Of Flight Diffraction (TOFD), which is an ultrasonic non-destructive technique, and naked eye observations. Statistical analysis is carried out to obtain the fatigue life associated with a 10% or 25% change of strain ranges measured on the top of the deck plate at crossbeam intersection, and the first visible crack on the top of the deck plate. Finite Element (FE) models are developed, and the Effective Notch Stress (ENS) is used to study the effect of the lack of penetration. The crack propagation path is analysed using fracture mechanics analysis by the eXtended Finite Element Method (XFEM). This study can be used in the technical specification “TS 1993-1-901 — Fatigue design of orthotropic bridge decks with the hot spot stress method” (in short TS) [24], which will be part of the second generation of Eurocodes.

2. Experimental investigation

2.1. Specimen

2.1.1. Geometric characteristic

A full-scale 9400 mm long and 5100 mm wide OBD has been constructed as the fatigue test specimen. Fig. 2 shows the geometric characteristics of the specimen. The specimen contains three crossbeams with a web thickness of 16 mm and a bottom flange of 200 mm wide and 12 mm thick. The 20 mm thick deck plate is supported by eight 6 mm thick trapezoidal-shaped stiffeners (sixteen C1c type welded details per crossbeam). The stiffeners are continuous at the crossbeams. The crossbeams are welded around four of the stiffeners, whereas the other four have an additional “Haibach” shape extended cut-out in the crossbeam [1,24]. Note that the cut-outs are not expected to influence the stress state of detail C1c under consideration. The deck plate is composed of two steel plates connected with a butt weld, which is

Table 1

Welding parameters used in the fabrication of the stiffener-to-deck plate connections.

Type	W1	W1	W2
Pass	1	2	1
Process	FCAW	SAW	SMAW
Wire diameter [mm]	1.2	3	4
Current [A]	230–240	520–530	160–170
Voltage [V]	25–27	25–57	23–24
Current type	DC+	DC+	DC+
Welding speed [cm/min]	42–48	45–50	8–10
Heat input [kJ/mm]	0.7–1.0	1.6–1.9	2.3–2.8

assumed not to affect the performance of detail C1c. The tested details are designated as SxS or SxN for the South or North sides of the stiffeners, respectively (see designations S and N in Fig. 2), where x denotes the stiffener number.

2.1.2. Welding procedure

The specimen is made from structural steel grade S355J2 with a nominal yield stress of 355 MPa [25]. It is known that the fatigue performance of welded connections may be affected by the welding process [26,27].

Two-pass automatic metal arc welding is used for welding S1, S3, S5, and S7 to the deck plate (denoted as Weld 1, in short W1), and single-pass manual metal arc welding is used for the other stiffeners (denoted as Weld 2, in short W2) to study the effect of the welding procedure on the fatigue performance. The stiffener end is bevelled to a flat edge prior to welding with a minimum thickness of 3 mm for W1. A lack of penetration of a maximum of 1.5 mm is specified for both welding procedures in line with [28], see Fig. 3. Table 1 gives the applied welding parameters. Non-destructive testing is executed and it is confirmed that the weld quality meets the required quality level, namely, quality level B of ISO 5871 [29].

Fig. 4 presents the resulting weld profiles at the representative cross sections. The geometry of the weld toe transition is an important factor affecting the fatigue resistance of weld toe cracks [28,30]. The flank angles of the automatic welding ($180^\circ - \theta'_A$ and $180^\circ - \theta''_A$) are typically smaller than those of the manual welded ones ($180^\circ - \theta'_M$ and $180^\circ - \theta''_M$). The weld surface of the automatic welding procedure appears smoother than the manual weld procedure.

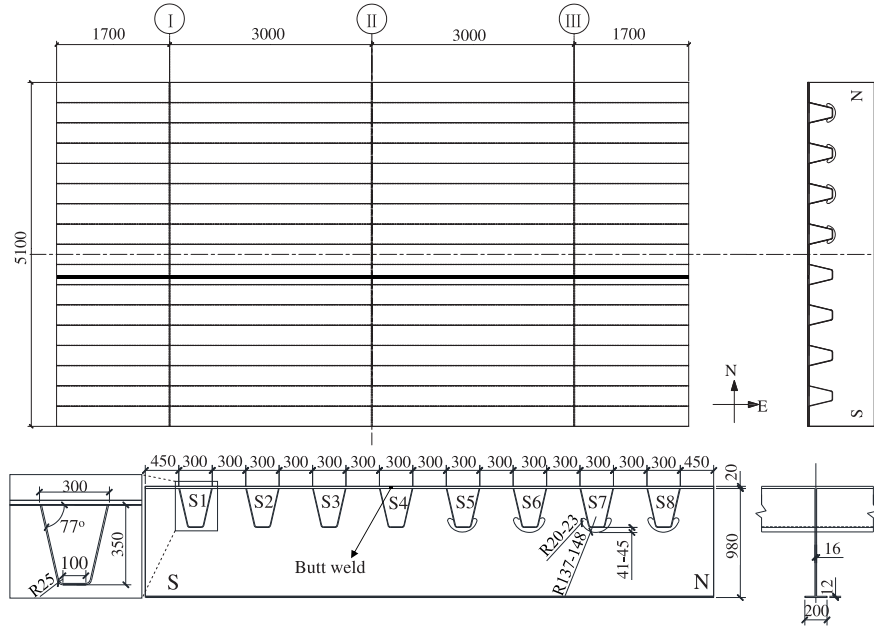


Fig. 2. Overview of the full-scale specimen (unit: mm).

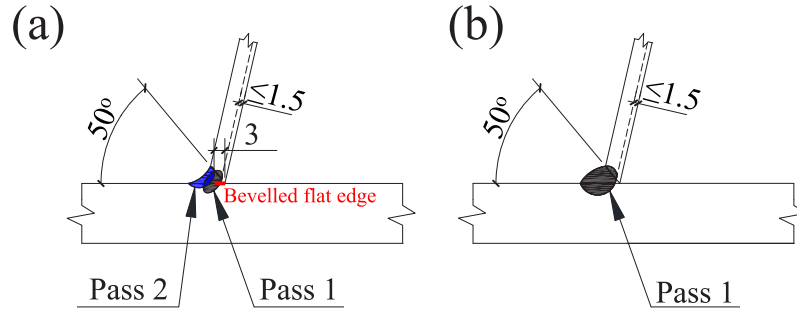


Fig. 3. Welding procedure of: (a) W1; (b) W2 (unit: mm).

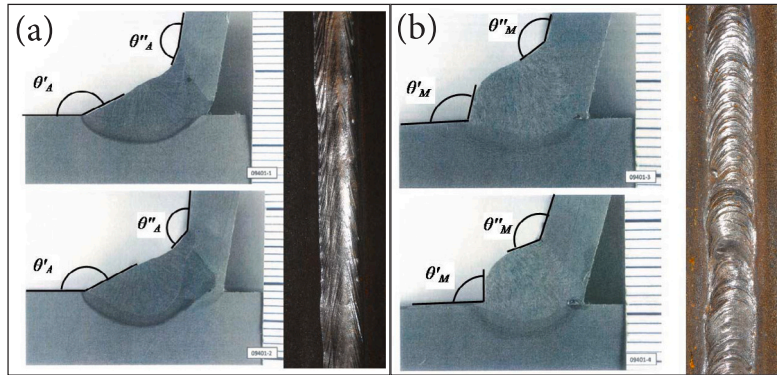


Fig. 4. Representative cross-sections of the stiffener-to-deck plate connections: (a) W1, and (b) W2.

2.2. Instrumentation

Electric resistance strain gauges are used to obtain the strain distribution in the direction perpendicular to the weld line of the deck plate near the detail of interest (detail C1c). Three sets of the strain gauges are symmetrically applied at both sides of the closed stiffeners,

as shown in Fig. 5. Set A (magenta) is applied at the top of the deck plate above every stiffener web. Set B (red) is applied at the top of the deck plate at S2 and S7. Set C (blue) is applied close to the weld root at the bottom of the deck plate of S6 and S7. The positions of strain gauges are selected sufficiently away from the weld to be unaffected by the local weld geometry and to measure global stress concentrations.

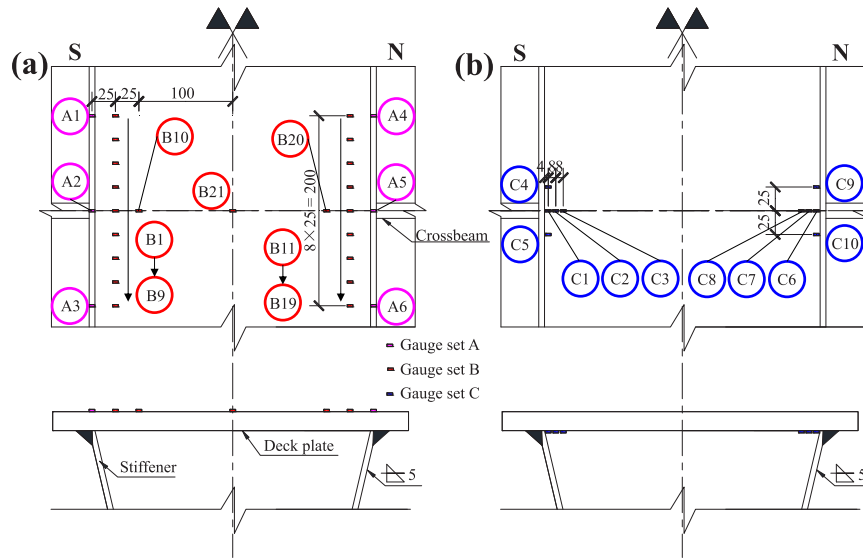


Fig. 5. The arrangement of strain gauges (unit: mm), (a) top of the deck plate, (b) bottom of the deck plate.

Table 2

Fatigue loading in the experimental programme.

ID		1	2	3	4	5	6	7	8
Phase 1	Maximum load [kN]	172	161	220	260	261	191	160	223
	Minimum load [kN]	2	16	20	24	24	27	16	23
	Load range [kN]	170	145	200	237	237	165	144	200
	Loading cycles [million]	5.1	12.5	5.1	1.2	5.0	5.3	19.1	5.6
Phase 2	Maximum load [kN]	190	161	220	264	264	196	162	220
	Minimum load [kN]	12	15	20	24	24	29	16	20
	Load range [kN]	178	146	200	240	240	168	146	200
	Loading cycles [million]	2.0	3.2	2.0	3.2	2.0	2.0	2.2	2.4

2.3. Fatigue loading programme

Fig. 6 shows a three-dimensional model of the setup and the specimen. The bottom flanges of the crossbeams are continuously supported on the concrete floor. The fatigue load is applied through a hydraulic actuator that presses onto a 32 mm thick steel plate and three plates of rubber, 8 mm thick each, see Fig. 7. The upper two rubber plates have a surface area of 270 mm × 320 mm. The lowest plate has a surface area of 180 mm × 320 mm, narrower than the other rubber plates, to allow the attachment of the strain gauges. The load is applied centred over one stiffener and one of the outer crossbeams. The load is shifted in each test to the adjacent stiffener. The strains in the deck plate at adjacent stiffeners are negligible, checked by strain gauge measurement. The load ratio, defined as the minimum load divided by the maximum load, is approximately 0.1. Each test contains two loading phases. The load is applied centred over the crossbeam in Phase 1, with four different levels of load ranges: 144 kN, 170 kN, 200 kN, or 240 kN to enable statistical analysis of the fatigue resistance. During Phase 1, no surface crack is detected on the deck plate from the top. In Phase 2, the loading area is shifted 100 mm to the east direction, away from the crossbeam. The load ranges in Phase 2 are nearly the same as in Phase 1. This load shift is considered relevant because it mimics the moving loads that bridges are subjected to (axles crossing the bridge in length direction). Section 3.1 provides the criterion to end Phase 1 and begin Phase 2 (see Table 2).

3. Experimental results

3.1. Fatigue crack characteristics

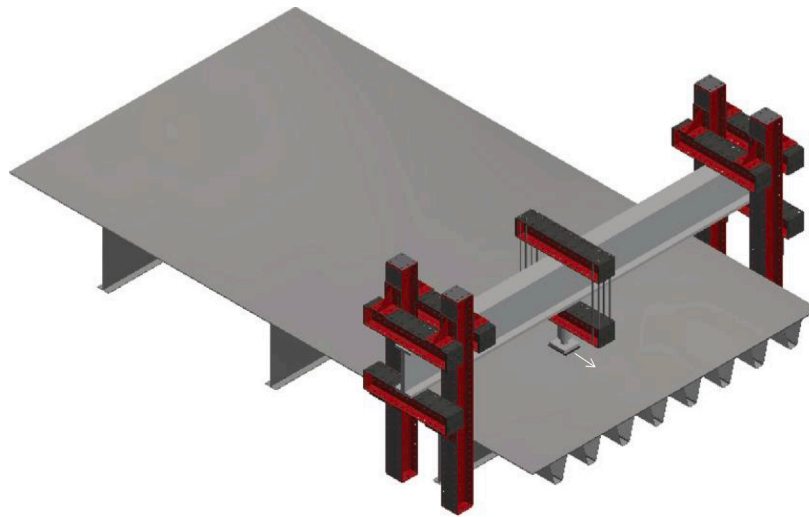
Visual inspections using naked eyes have been carried out at the end of Phase 1 and Phase 2 on the top of the deck plate for back surface

breaking cracks detection. Cracks are not found on the top of the deck plate at the end of Phase 1. One back surface breaking crack is detected on the south side of S4 at the end of Phase 2, shown in Fig. 8. A 136 mm long arc-shaped crack is shown on S4S. The blue dash lines represent centrelines of the crossbeam and the stiffener webs. Note that only a portion of the loading area in Phase 2 is displayed in Fig. 8.

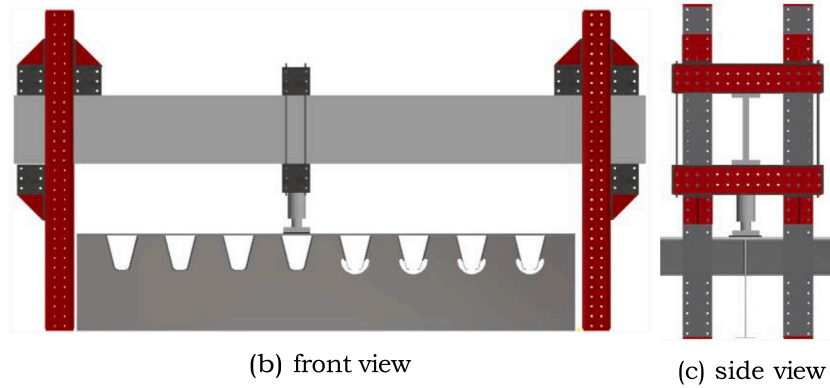
TOFD measurements have been carried out within an approximate distance of 450 mm on either side of the crossbeam using the dB-UT system [31]. Fig. 9 shows an illustration of TOFD measurements. The ultrasonic signal is sent and received from the top of the deck plate. Diffracted and reflected signals occur when the ultrasonic signals meet a crack. The signal receiver receives the diffracted signals. Details about the TOFD procedure are given, e.g., in [32].

Fig. 10a shows the inspected regions of the TOFD measurements. The scan device moves stably from one side of the crossbeam to the other, with the position automatically stored in the system. The blue and red lines (separated manually with the intention of a better visualisation) represent detected cracking areas at the end of Phases 1 and 2, respectively. Fig. 10b gives a typical example of the signals in the presence of a crack. The centreline of the crossbeam is defined as a distance of 0, and negative numbers indicate the west direction.

Table 3 summarises the detected cracks. Phase 1 is terminated (and Phase 2 starts) after reaching 5 million cycles in most tests. The TOFD measurements reveal that cracks developed in an early stage in Phase 1 in most tests, whereas these hardly grow (or are arrested) during the last million cycles of Phase 1. Phase 1 is terminated after a much larger number of cycles in tests 2 and 7 to determine whether the cracks will pick up growth in a later stage. Phase 1 is terminated earlier in test 4 to determine if this will affect the growth in Phase 2. The largest cracks arrest at a depth of approximately 14 mm to 15 mm (75% of the deck plate thickness) at the end of Phase 1. The start and end positions reveal that the crack may not propagate symmetrically at two sides of the crossbeam, which is not surprising given the random nature of the fatigue process and the weld imperfection distribution. Besides the main crack, secondary cracks are detected at various details. The cracks grow in the length direction in Phase 2 (especially for S4S-01, S6S-02, and S7S-01) but, with two exceptions, they hardly grow in the depth direction and none of the cracks grow through the thickness. Note that the start and end positions of the cracks may not be accurately located when the cracks are small, e.g., S3S-01. A thorough visual inspection of the entire specimen is executed at the end of Phase 2. In addition to C1c, three other types of cracks are detected, as shown in Fig. 11. Fatigue cracks are found in the base material at the bottom of the deck



(a) global view, with the arrow showing the direction of the load shift in Phase 2



(b) front view

(c) side view

Fig. 6. Sketch of the setup frame and actuator.

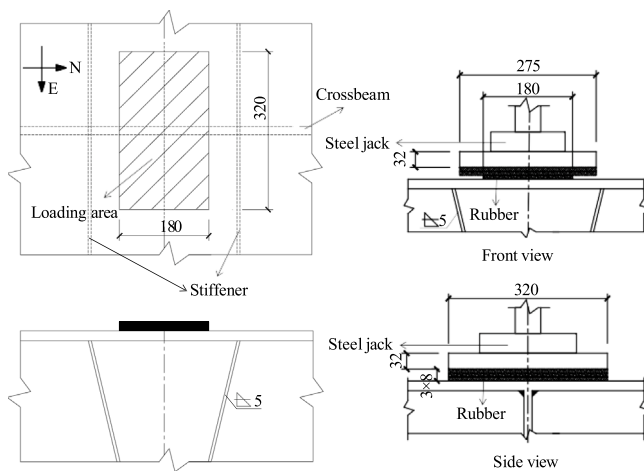


Fig. 7. Illustration of the load position and region in Phase 1 (unit: mm).

plate with a certain distance from the weld toe (Fig. 11a), in the weld and in the stiffeners (Fig. 11b), at the lower part of the stiffener-to-crossbeam connections of S1S, S2S, and S2N, on both free edge and in span sides (Fig. 11c). A summary of the deck plate cracks other

than type C1c detected at the bottom of the deck plate is presented in Table 4. S1 and S8 have been cut for other studies before the inspections are performed. Therefore, no information is available for S1 and S8. It is unknown whether the first two types of cracks are secondary (i.e. occurring as a result of the C1c type cracks).

The appearance of a crack can be shown by a change in recorded strain ranges during a fatigue test. An evaluation criterion often applied in fatigue testing of OBD details is a certain change of strain ranges as a function of the applied number of cycles.

Fig. 12 shows the strain ranges of the gauges at the top and the bottom of the deck plate around the crossbeam, as a function of the logarithm of the number of cycles for S6 and S7 with the markers indicating the 10% (first symbol) and 25% (second symbol) changes of each curve. The strain ranges are approximately constant up to 0.1 million cycles, indicating that there is no significant settlement effect. The drop in strain range, in some cases preceded by an increase in strain range, is attributed to the development of cracks. An immediate drop in reading may indicate a crack very close to the strain gauge, while an initial increase may indicate a crack initiating at a distance from the gauge. Fig. 13 shows the strain ranges at the top of the deck plate, at and within 100 mm distance from the centreline of the crossbeam. The change in strain range takes place over a large number of cycles. It indicates that a fast initiation followed by a relatively slow propagation in line with the observations from thinner deck plates [1,2,9,12]. This finding from strain ranges agrees well with the TOFD measurements [33] and fracture mechanics calculations [13], where a slow propagation is also observed.

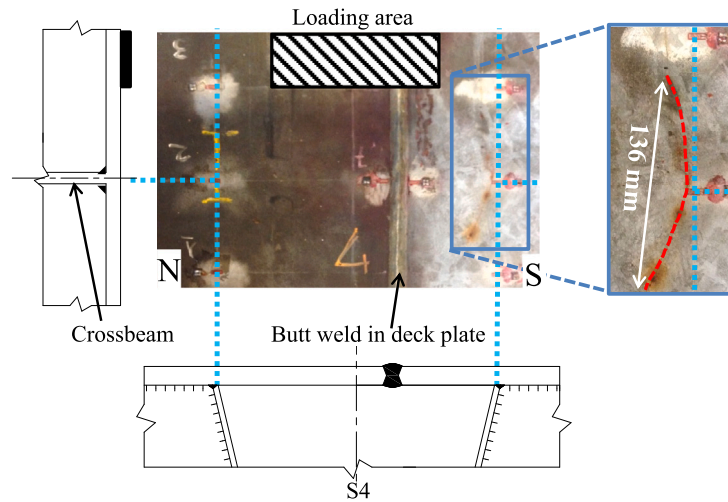


Fig. 8. The visible cracks observed from the top of S4 at the end of Phase 2.

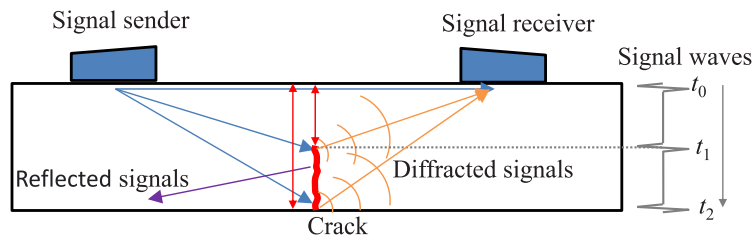


Fig. 9. Illustration of the ultrasonic signals in TOFD measurement.

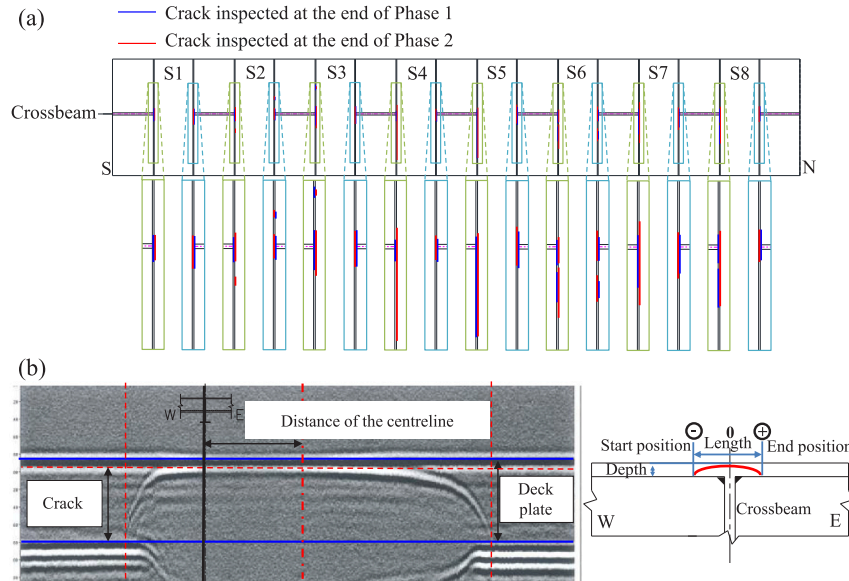


Fig. 10. TOFD measurements for detail C1c, (a) inspection region, (b) an example at S7S (the ultrasonic signal waves on the left and the illustration on the right) [31].

3.2. (Structural) hot spot stress at the initial loading stage

High stress concentrations appear in many details of OBD, including detail C1c. Due to the large stress gradients, the nominal stress is not simply defined for detail C1c. The hot spot stress method provides an attractive alternative for structural stress calculation at the positions of interest. De Jong [34] proposed a simplified calculation model for the hot spot stress of detail C1c. It considers a 2D representation of the deck plate, which is modelled as a beam fully clamped at the intersections

with the crossbeam, and it employs the stress at the bottom of the beam, see Fig. 14. The “tyre load” with a contact area of $L_q \times W_q$ is modelled with a uniformly distributed load q and L_d is the distance between the stiffener webs (i.e., the unsupported span of the deck plate). A slightly modified version of this hand calculation model is employed in the Dutch National Annex to NEN-EN 1993-2+C1/NB: 2012 [35]. It is assumed that the load acts at the deck plate centre at a spread angle of 45° . Thus, q can be determined with Eq. (1) [34] where ΔF and t_d are the tyre load and the thickness of the deck plate, respectively.

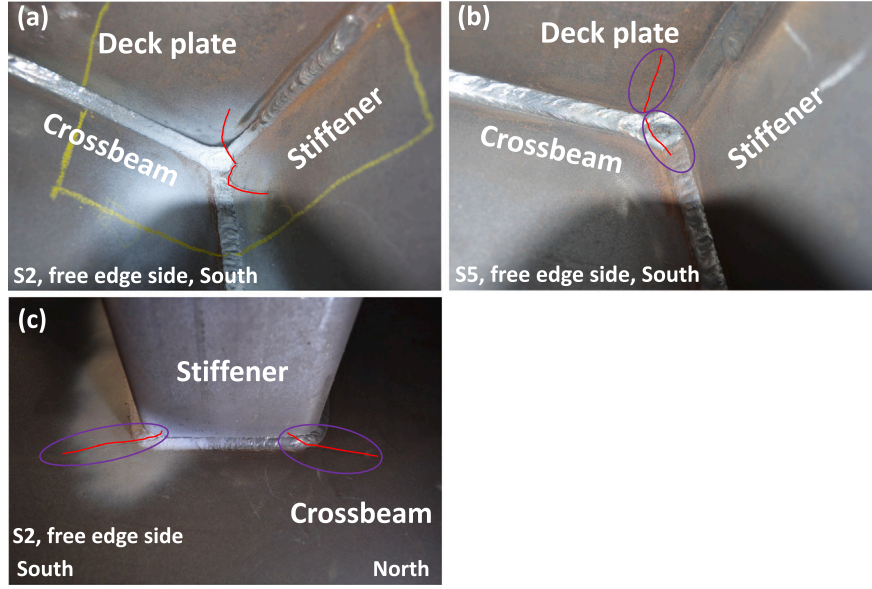


Fig. 11. Fatigue cracks other than type C1c observed from the bottom of the deck plate and stiffener-to-crossbeam at the end of Phase 2.

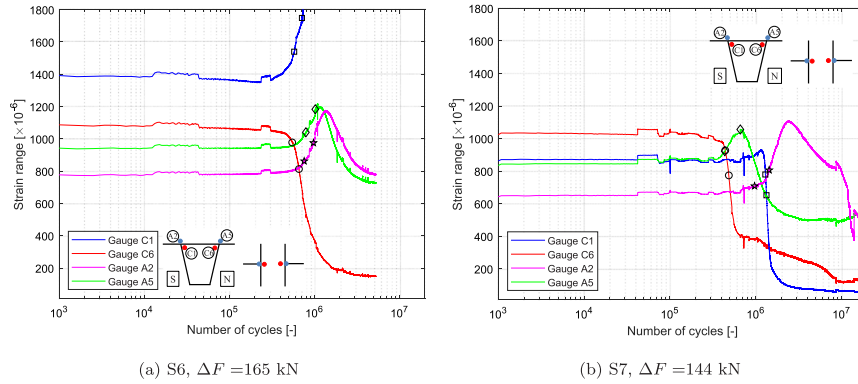


Fig. 12. Change of strain ranges as a function of the applied number of cycles.

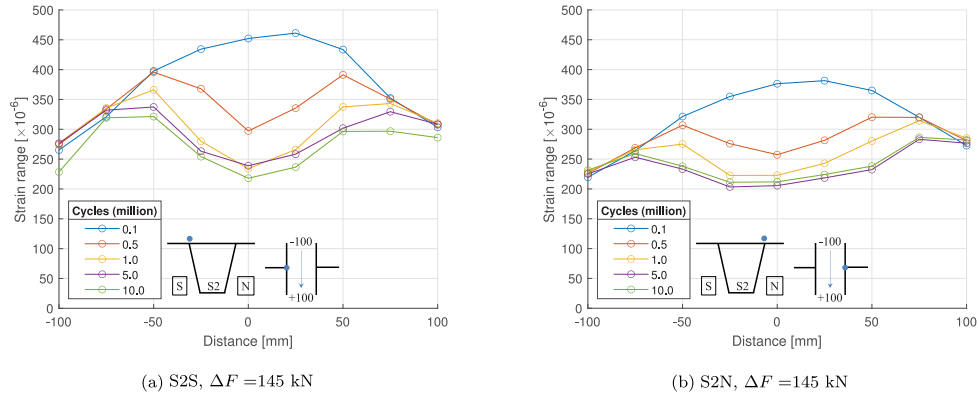


Fig. 13. The distribution of the strain ranges on the top of the deck plate at the selected cycles.

The hot spot stress range $\Delta\sigma_{hs}$ is determined as the nominal stress from the simplified beam model (shown in Fig. 14), $\Delta\sigma_{nom}$, multiplied by a stress concentration factor (SCF), see Eqs. (2) to (4) [34,35]. $\Delta\sigma_{nom}$ is calculated using beam theory. The SCF is based on a curve fit of parametric 3D analyses using the FE analyses, accounting for the difference in the effect of the crossbeam between the 3D reality

and the 2D beam models. The following dimensions are applied for the full-scale specimen presented in the current paper: $t_d = 20$ mm, $L_q = 180$ mm, $W_q = 320$ mm, and $L_d = 300$ mm. This results in a hot spot stress of $\Delta\sigma_{hs} = 156.42$ MPa for a load range of 100 kN. Note that the model may not be accurate in special cases with significant shear deformation of the crossbeam, which is different from the current

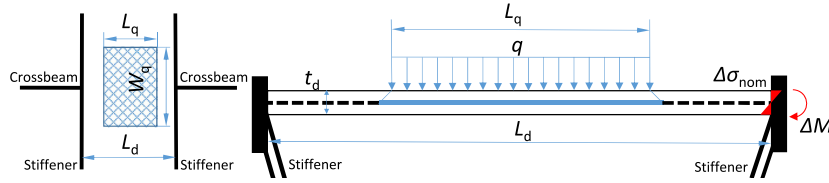


Fig. 14. Illustration of the hand calculation model for $\Delta\sigma_{hs}$ in NEN-EN 1993-2+C1/NB: 2012 [35].

Table 3

Fatigue cracks positions of detail C1c at the end of Phases 1 and 2 as obtained by TOFD measurements (unit: mm).

ID	Start position		End position		Length		Depth	
	1	2	1	2	1	2	1	2
S1N-01	-38	-40	78	78	116	118	14.5	15.1
S1S-01	-42	-42	54	48	96	90	14.1	14.9
S2N-01	-124	-130	-99	-103	25	27	2.1	2.2
S2N-02	-38	-44	47	42	85	86	14.9	15.5
S2S-01	-266	-260	-266	-260	0	0	2.4	2.3
S2S-02	-34	-50	55	52	89	102	14.6	15.1
S2S-03	-	106	-	138	-	32	-	4.3
S3N-01	-57	-55	72	73	129	128	14.5	15.3
S3S-01	-212	-202	-172	-180	40	22	6.2	6.4
S3S-02	-58	-57	84	104	142	161	14.6	15
S4N-01	-26	-38	56	49	82	87	14.7	14.8
S4S-01	-24	-66	53	335	77	401	13.7	20
S5N-01	-51	-68	79	70	130	138	13.7	14.5
S5S-01	-34	-46	323	320	357	366	19.5	19.5
S6N-01	-31	-54	53	53	84	107	14	14.7
S6N-02	125	104	185	198	60	94	3.9	11.3
S6S-01	-22	-32	68	61	90	93	13.6	14.4
S6S-02	92	76	199	254	107	178	13.8	14.4
S7N-01	-39	-48	98	116	137	164	14.3	14.6
S7S-01	-37	-86	149	211	186	297	14.3	15.8
S8N-01	-56	-56	53	59	109	115	13.7	13.9
S8S-01	-39	-52	63	58	102	110	13.8	13.8
S8S-02	82	58	220	215	138	157	13.8	14.3

Table 4

Summary of the fatigue cracks other than type C1c observed from the bottom of the deck at the end of Phase 2.

	S1		S2		S3		S4		S5		S6		S7		S8	
	S	N	S	N	S	N	S	N	S	N	S	N	S	N	S	N
Free edge	-	-	x		x	x	x		x	x	x		x		-	-
In span	-	-	x					x	x	x	x	x	x	x	-	-

set-up with continuously supported crossbeams.

$$q = \frac{\Delta F}{(W_q + t_d) \times (L_q + t_d)} \quad (1)$$

$$\Delta\sigma_{nom} = \frac{\Delta M}{I} \quad (2)$$

where ΔM is the bending moment range and the second moment of area $I = t_d^3/12$.

$$\Delta\sigma_{hs} = SCF \cdot \Delta\sigma_{nom} \quad (3)$$

$$SCF = \begin{cases} 1.4 & \text{pavement} \geq 50 \text{ mm,} \\ 1.2957 - 0.00938 t_d & \text{pavement} < 50 \text{ mm.} \end{cases} \quad (4)$$

3.3. Evaluation of the experimental results

3.3.1. Fatigue life evaluation criteria

Various fatigue life evaluation criteria have been proposed in the literature for detail C1c. Some authors used the number of cycles at a certain change of strain ranges at the top side of the deck plate as the evaluation criterion: 10% (Kolstein [1]), 15% (Dung et al. [36]), 20% (Konda et al. [12]), and 25% (Kolstein [1]).

Table 5

Experimental results of Phase 1.

ID	ΔF [kN]	$\Delta\sigma_{hs}$ [MPa]	N_1	N_2	N_t	N_2/N_1	N_t/N_1
S1N	170	252	203 000	489 797	5 102 664	2.5	25.1
S1S	170	252	438 837	729 878	5 102 664	1.7	11.6
S3N	200	296	127 137	176 034	5 088 787	1.4	40.0
S3S	200	296	236 629	339 841	5 088 787	1.4	21.5
S5N	237	351	158 904	233 896	5 000 001	1.5	31.5
S5S*	237	351	1 295 773	5 000 001	5 000 001	3.9	3.9
S7N	144	213	438 119	663 105	19 122 751	1.5	43.7
S7S	144	213	974 245	1 440 261	19 122 751	1.5	19.6
S2N	145	215	211 877	337 779	12 514 488	1.6	59.1
S2S	145	215	235 858	686 318	12 514 488	2.9	53.1
S4N	237	351	382 160	612 537	1 225 001	1.6	3.2
S4S	237	351	142 185	341 964	1 225 001	2.4	8.6
S6N	165	244	797 706	1 029 209	5 287 737	1.3	6.6
S6S	165	244	757 172	978 800	5 287 737	1.3	7.0
S8N	200	296	126 363	188 983	5 603 231	1.5	44.3
S8S	200	296	169 902	328 062	5 603 231	1.9	33.0

Another criterion used to evaluate the fatigue performance of detail C1c is the number of cycles at the earliest detection (with naked eyes) of a through-thickness crack at the top side of the deck plate, denoted here as N_3 [1,2,33]. This failure criterion is widely adopted for OBD tests because of the relatively slow crack propagation and the ability to still carry the load with a limited surface breaking length. This failure criterion is more practical for on-site inspections, and it is adopted in the TS [24,28].

3.3.2. Statistical analysis

Statistical analysis is employed to evaluate the fatigue resistance of detail C1c tested in the current paper and the results collected in the literature. The Basquin relation describes the relationship of the number of cycles N_R and the applied stress range $\Delta\sigma$:

$$\log N_R = \log a - m \cdot \log \Delta\sigma_C \quad (5)$$

The characteristic fatigue resistance, $\Delta\sigma_C$, is defined as the stress range at 2 million cycles with 95% exceedance fraction and the slope parameter, m , is fixed to 3 (fully informative prior). This corresponds to the definition used in (pr)EN 1993 [15,16,24] following the statistical analysis described in [37,38].

3.3.3. Current experiment with a 20 mm thick deck plate

Table 5 presents the experimental results of Phase 1. The number of cycles corresponding to strain range changes, N_1 and N_2 , and the total load cycles, N_t , are listed. The ratio N_2/N_1 evaluated from the strain gauges at the top of the deck plate ranges between 1.3 and 2.9. A slow crack propagation is observed as the ratio N_t/N_1 varies from 3.2 to 59.1. The wide range in numbers may be caused by the crack sizes (shown in Table 3) at the end of loading. S5S (marked) is excluded from the statistical analysis. This is because the strain range change was first observed at the position 100 mm away from the centre line of the crossbeam for this location. The crack may not initiate at the crossbeam location.

Fig. 15 shows the results of the statistical analysis for the evaluation criteria of 10% and 25% change of strain range. The numbers in the graphs present the fatigue resistances with 5%, 50%, and 95%

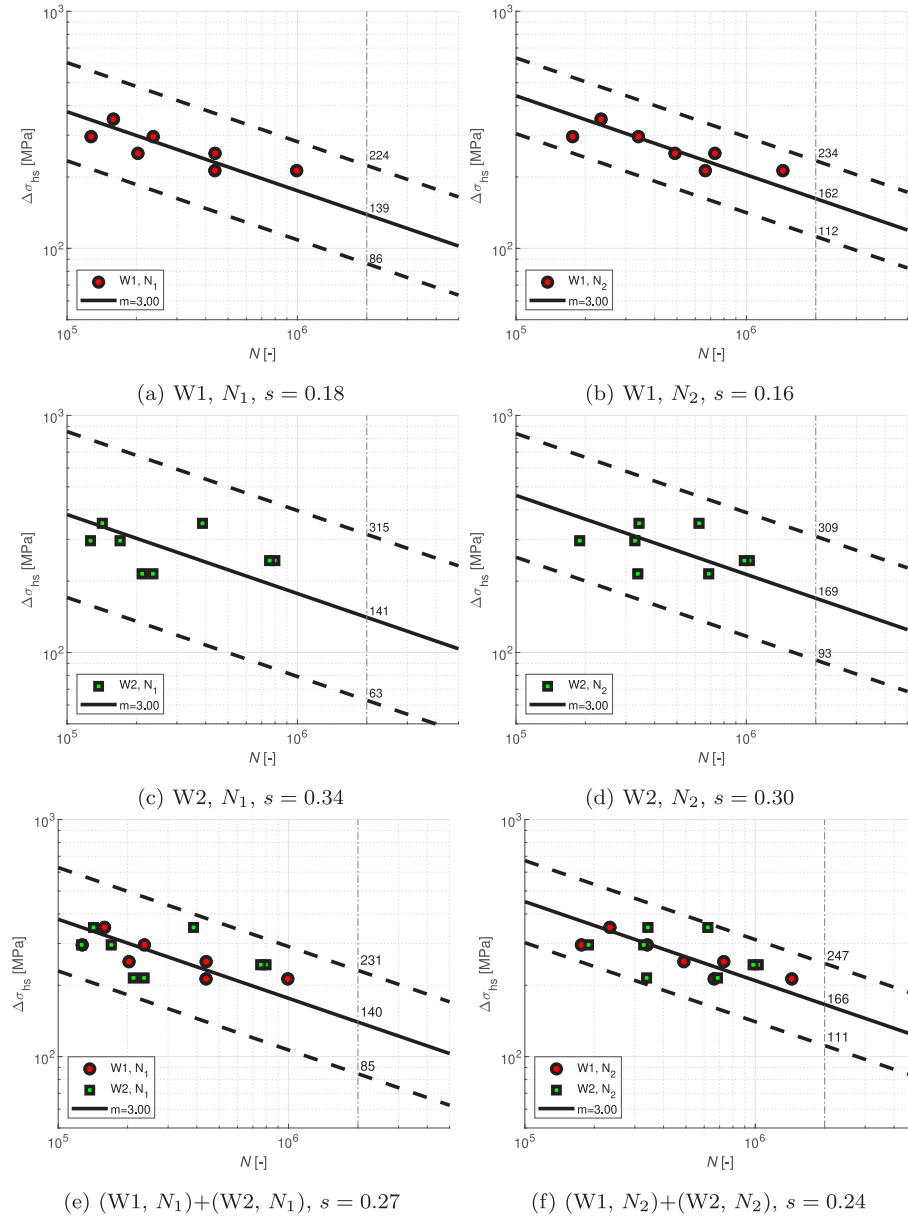


Fig. 15. Statistical analysis of the experimental results with a 20 mm thick deck plate.

exceedance fractions. The fatigue resistances with 50% exceedance fraction of W1 and W2 are approximately equal, while the standard deviation (s) of W1 (0.16 to 0.18) is smaller than W2 (0.30 to 0.34), resulting in a lower value of $\Delta\sigma_C$ for W2. Combining W1 and W2, $\Delta\sigma_C$ values are 85 MPa and 111 MPa with the standard deviations of 0.27 and 0.24 for N_1 and N_2 , respectively.

3.3.4. Experiments with long load patches

Fig. 16 gives experimental data from the current study and the literature with thinner deck plates ($t_d = 10$ or 12 mm). All data are obtained with load patches with $W_q = 320$ mm (dedicated as long load patches). The fatigue resistances with 50% and 5% exceedance fractions of the joint dataset are approximately equal to those of the 20 mm deck plate sub-dataset for criterion N_1 and they are slightly higher for N_2 . The characteristic resistances related to N_1 and N_2 , are 86 MPa and 117 MPa, respectively. They are (almost) equal to the characteristic resistances given in the standards AASHTO-LRFD Bridge Design Specifications: 2012 [19] (Category C, $\Delta\sigma_C = 90$ MPa) and the

Dutch National Annex to EN 1993-2: 2012 [35] ($\Delta\sigma_C = 125$ MPa), respectively. The characteristic fatigue resistance for criterion N_3 is $\Delta\sigma_C = 167$ MPa, obtained from the sub-dataset with thin deck plates only because (almost) no back surface breaking cracks are not observed for thick deck plates. Note that the characteristic fatigue resistance found for N_3 is much higher than the hot spot stress fatigue resistances for weld toe cracks recommended by IIW [7] and in (pr)EN 1993-1-9 [15,16]. Both documents give $\Delta\sigma_C = 100$ MPa for weld toe cracks at non-loaded fillet welds. Maljaars et al. [13] give possible reasons for the relatively high resistance of detail C1c:

- Whereas fatigue cracks in welded connections usually either initiate from the plate and propagate in the base metal or initiate from the root and propagate in the weld, the crack in detail C1c initiates from the root and propagates in the base metal. It is, hence, a different type of crack.
- The fatigue resistance in the standards is (conservatively) given for tension–tension loading, where detail C1c is subject to bending of the deck plate.

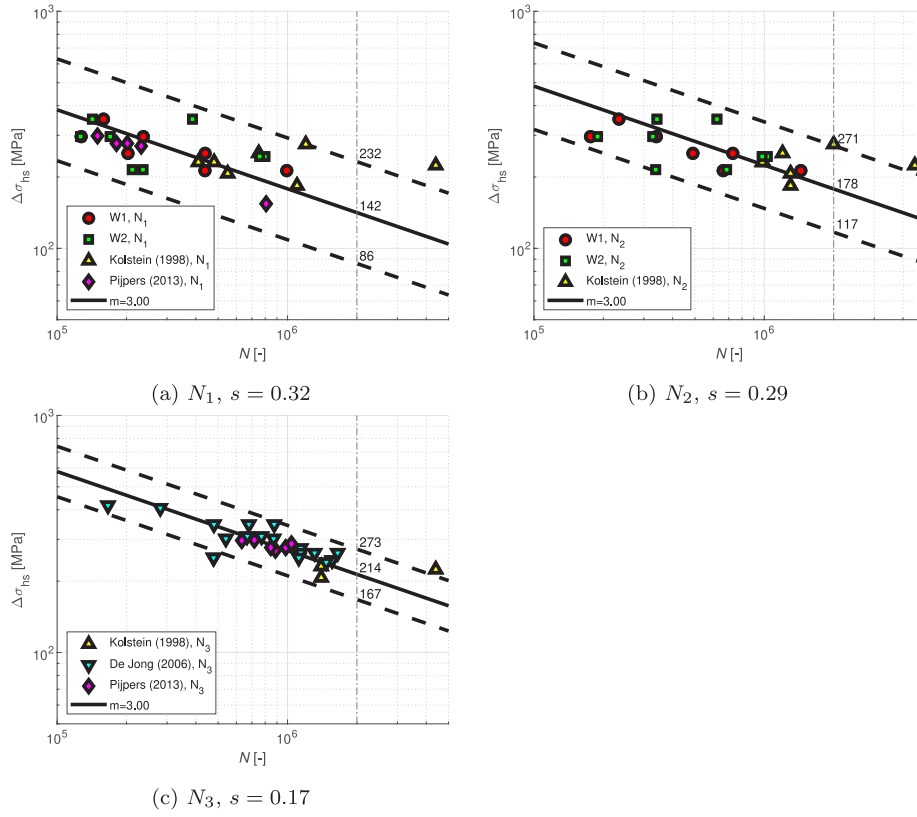


Fig. 16. Statistical analysis for the joint database using long load patches [1,2,33].

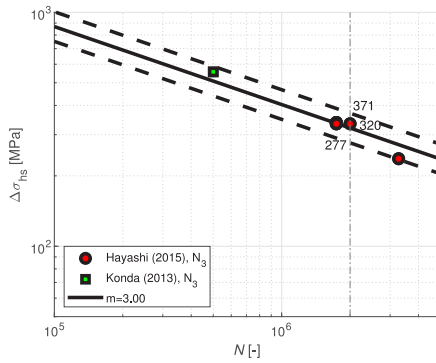


Fig. 17. Statistical analysis for the specimens loaded using short load patterns (N_3 , $s = 0.09$) [9,12].

- A load shedding effect occurs for detail C1c, where the stress reduces with the distance from the crossbeam. This gives a lower propagation rate as compared to usual details.

3.3.5. Experiments with short load patches

In [9,12], experimental investigation was executed but using shorter load patches with a size of 260 mm × 200 mm for 12 mm deck plates, and 200 mm × 200 mm for 12 mm or 16 mm deck plates, respectively. Surface cracks were found only in the specimens with 12 mm deck plates. Fig. 17 shows the statistical analysis for the specimens loaded using short load patches. The hot spot stress ranges are obtained by

the FE calculation (validated by the strain gauge measurements) using the surface extrapolation approach in TS [24]. This is because the specimens in [9,12] are approximately 300 mm wide and the hand calculation model has not been verified for this type of specimen. High fatigue resistance, $\Delta\sigma_C = 277$ MPa, is observed, which is even higher than the values of long load patches. The FE calculation in Section 4 explains the difference: The maximum principal stress (in absolute value) decays faster with the distance from the centrelines of the crossbeam for short load patches compared to the long load patches.

4. Finite element analysis

4.1. Description of the model

Fig. 18 shows an overview of the FE model generated and analysed with the commercial FE software Abaqus 2019 [39], dedicated to simulating Phase 1. A symmetrical model is built to reduce the computational cost, see Fig. 18. Symmetry in the z-direction is not used to study Phase 2, which is not further discussed here. The FE model is 1300 mm long, and it contains one-and-a-half closed stiffeners. A “Static” load step is employed with the implicit calculation method [39]. The bottom side of the lower flange is constrained in the vertical displacement direction ($U_Y=0$). The symmetry boundary conditions with $U_X=0$ for Sides 1 and 2, and $U_Z=0$ for Sides 3 and 4. Note that a sensitivity study has been executed using different boundary conditions for Sides 1, 3, and 4, varying these boundaries from free of constraints to fully constrained in all directions with no noticeable effect on the local stress at the hot spot. The results given below are based on the symmetry boundary conditions at the four side planes. A uniform pressure load is applied at the tyre contact surface of Phase 1. The linear elastic material is applied in the model with Elastic modulus $E_s = 210$ GPa and Poisson’s ratio $\nu_s = 0.3$. Second-order brick elements with reduced integration (type C3D20R [39]) are employed

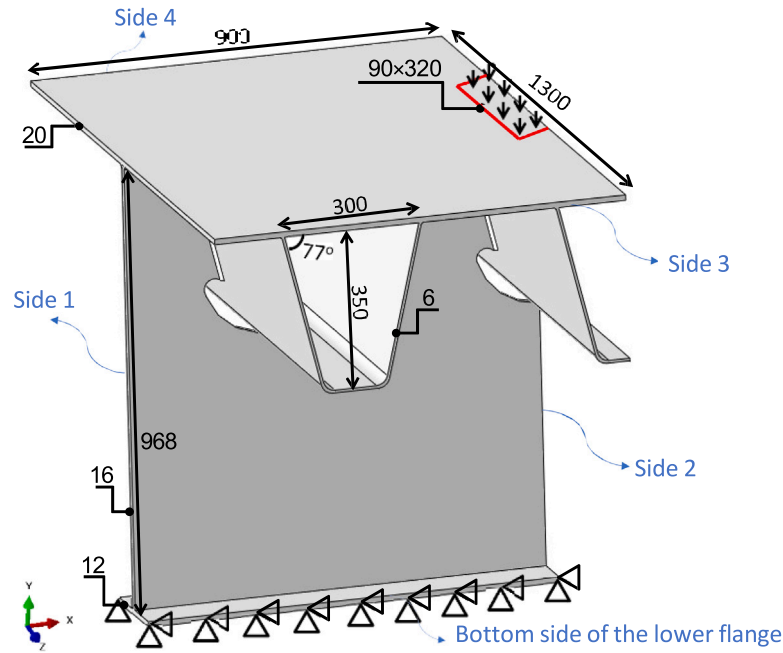


Fig. 18. Overview of the FE model (unit: mm).

with a locally refined mesh (see Fig. 19 for the nodal positions shown as markers).

4.2. Model validation

Fig. 19 shows the strain ranges from the experimental measurements and FE calculation. The values are normalised to a load range of 1 kN. The strain ranges at the top of the deck plate increase from 2×10^{-6} to 3×10^{-6} with the position approaching the crossbeam, Fig. 19b. The results of the FE calculation are close to the average values from experiments. Overall, the FE model gives a reasonable agreement with the experimental data both qualitatively and quantitatively.

4.3. Local stress state

The ENS [7,16] is applied to study the local stress state at the weld root. Fig. 20 shows the same FE model as shown in Fig. 18, but with two sub-regions with a denser mesh, Sub 1 and Sub 2. Tie constraints are employed at the interfaces [39] between the sub-regions and the global model. The approximate element sizes in the global, Sub 1, and Sub 2 regions are $50 \times 50 \times 50 \text{ mm}^3$, $8 \times 8 \times 8 \text{ mm}^3$, and $0.5 \times 0.5 \times 0.5 \text{ mm}^3$, respectively. Four models are constructed with a lack of penetration adopted in the Sub 2 region of 0.0 mm, 0.5 mm, 1.0 mm, and 1.5 mm. The ENS at the weld root is modelled with a 1 mm radius notch with following the IIW recommendations [7]. Fig. 21 shows the principal (in absolute value) and the von Mises stresses around the notches under the normalised load of 1 kN at the crossbeam conjunction. The minimum principal and maximum von Mises ENS values range from -7.8 to -7.6 MPa (from 4.9 to 5 times of $\Delta\sigma_{hs}$ in absolute value) and from 6.8 to 7.0 MPa (from 4.3 to 4.5 times of $\Delta\sigma_{hs}$), respectively. This indicates that a lack of penetration ranging between 0 to 1.5 mm has no significant effect on the ENS, similar to the findings in [36] for a 12 mm thick deck plate. The low sensitivity at the resistance to the local weld geometry, as determined by the ENS, may also explain the low sensitivity to the welding process observed in the experiments. Fig. 22 compares the principal stress (in absolute value) distribution loaded with different patch sizes. A long load patch ($90 \times 320 \text{ mm}^2$) results in a more uniform stress distribution (smaller peak stress at the weld root in conjunction with crossbeam position) than a short load patch ($90 \times 200 \text{ mm}^2$).

See Fig. 23 for the principal stress (in absolute value) of two selected paths, Path 1 or 2 at the bottom of the deck plate with the direction along the longitudinal weld at distances of 2.2 mm or 4.4 mm from the weld root, and the ratio of principal stress between the short ($90 \times 200 \text{ mm}^2$) and the long patch ($90 \times 320 \text{ mm}^2$).

4.3.1. Fracture mechanics analyses of crack shapes

Further FE analyses are conducted to evaluate crack arrest and crack propagation paths. The fracture mechanics method using the XFEM has been employed to study crack propagation. Four models with 10 mm, 12 mm, 16 mm, and 20 mm thick deck plates are created as presented in Fig. 20. Here, the global and Sub 2 regions are meshed using the first-order brick element with reduced integration (C3D8R) and Sub 2 is activated as the enriched region for the XFEM [39]. Two load patches with the sizes $270 \times 320 \text{ mm}^2$ (for the 12 mm deck plate) and $180 \times 320 \text{ mm}^2$ (for other deck plate thicknesses) are applied. A semi-circular-shaped crack is inserted at the weld root with a horizontal shift of 0.3 mm from the weld root to avoid singularity, see Fig. 24. The depth and semi-length of the initial crack are $a = 0.5 \text{ mm}$ and $c = 0.5 \text{ mm}$, based on the detectability of flaws [40], respectively. The initial angle assumed between the crack plane and the vertical direction, θ , is 0° for 10 mm and 12 mm deck plate [13], and 30° for 16 mm and 20 mm deck plate [14] following observed crack shapes. The Virtual Crack Closure Technique (VCCT) is employed to calculate the strain energy release rate [39]. The element breaks at the maximum value position in each increment with the propagation direction following the Maximum Tangential Stress (MTS) criterion, see Eq. (6) where $\hat{\theta}$ is the crack propagation angle [39]. Cyclic loading is applied in a “low-cycle fatigue analysis” step with the modified Paris’ equation for the strain energy release rate. The material properties are $m = 3$ (dimensionless), $C = 1 \times 10^{-13}$, and $\Delta K_{th} = 63$ (conservative value) with units in millimetres and Newton following [7,13]. Tensile residual stresses are assumed at the weld root of the stiffener-to-deck plate connections, and the crack is assumed to remain open during the entire load cycle [13]. This study focuses only on the fatigue crack propagation shapes and the crack arrest phenomenon using linear elastic fracture mechanics. The applied forces are high enough ($\Delta\sigma_{hs}$ between 200 MPa and 250 MPa) to propagate the crack at the initial state, while the fracture toughness

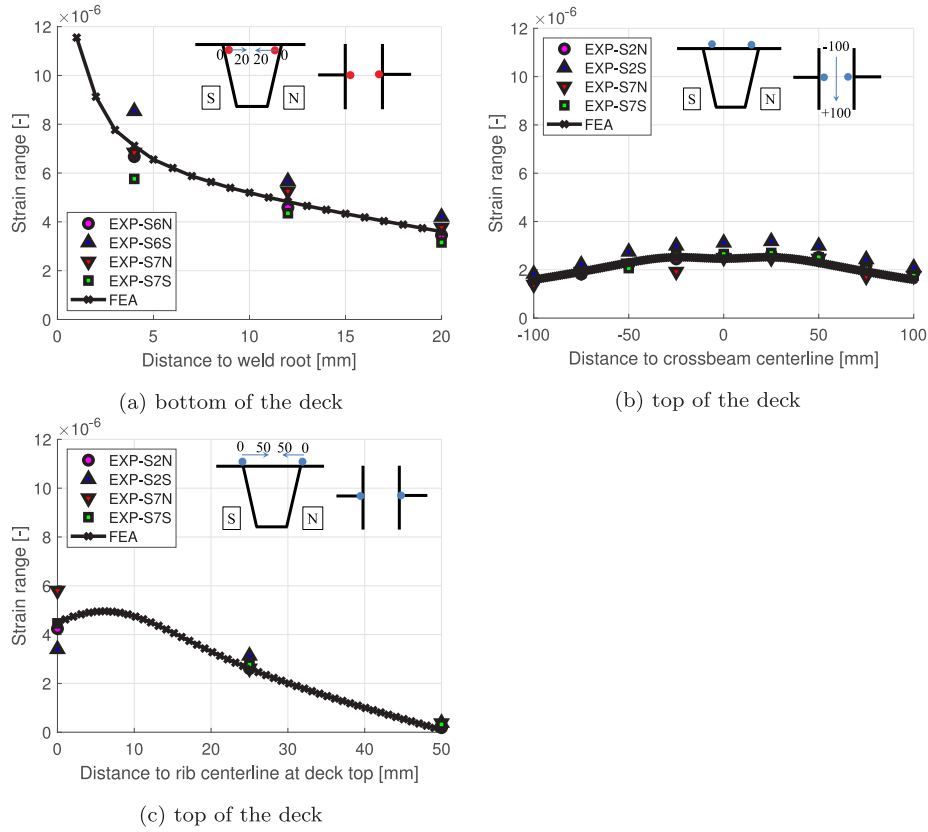


Fig. 19. Comparison of the experimental measurements and FE calculation under the normalised 1 kN load range.

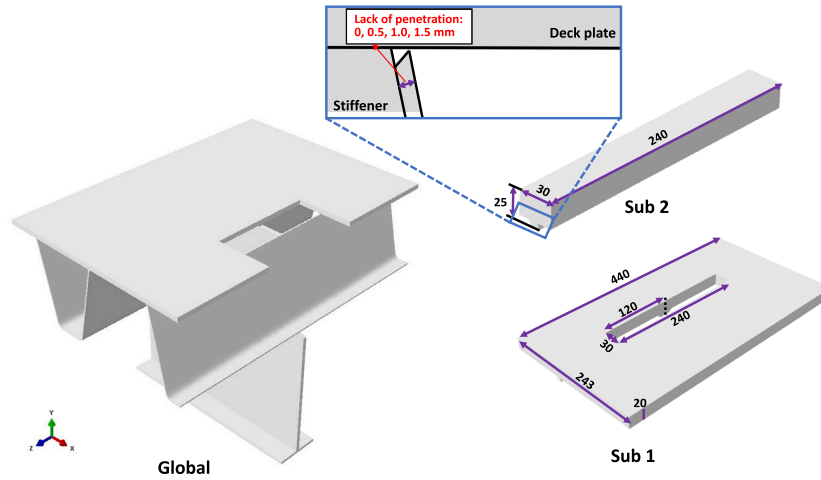


Fig. 20. Illustration of the FE model with global and sub-regions (unit: mm).

is not considered. Local plastic failure is excluded from the analysis. A fatigue life calculation can be done using the XFEM [41], which is left out of the scope of the current paper.

$$\hat{\theta} = \arccos \left(\frac{3K_{II}^2 + \sqrt{K_I^4 + 8K_I^2 K_{II}^2}}{K_I^2 + 9K_{II}^2} \right) \quad (6)$$

Fig. 25 illustrates the crack shapes of the four simulations. A three-dimensional crack with a shape close to the semi-elliptical is observed for all deck plate thicknesses. The crack propagates in depth and length direction until it breaks through the top surface of the deck plate in the 10 mm thick deck plate simulation (defined as failure type 1). Crack arrest is predicted for the 12 mm thick deck plate simulation but very close to the top surface (defined as failure type 2). It then

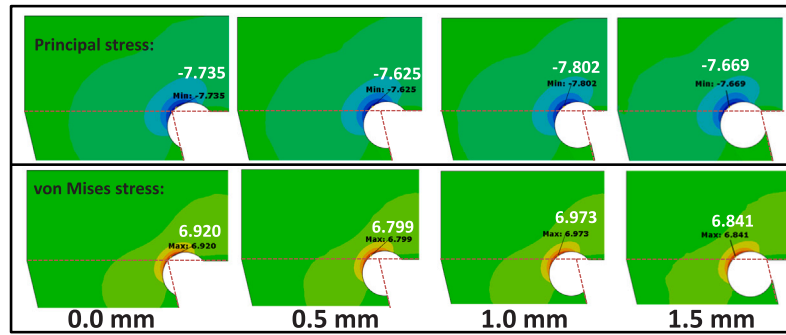


Fig. 21. ENS of weld root at the crossbeam with different lack of penetrations under the normalised load of 1 kN.

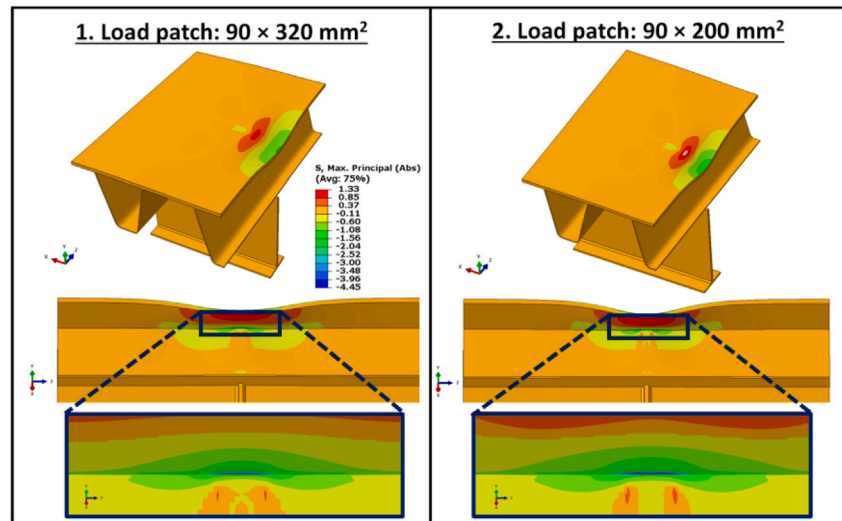


Fig. 22. Principal stress distribution under the normalised load of 1 kN loaded with different patch widths (deformation scale: 20000).

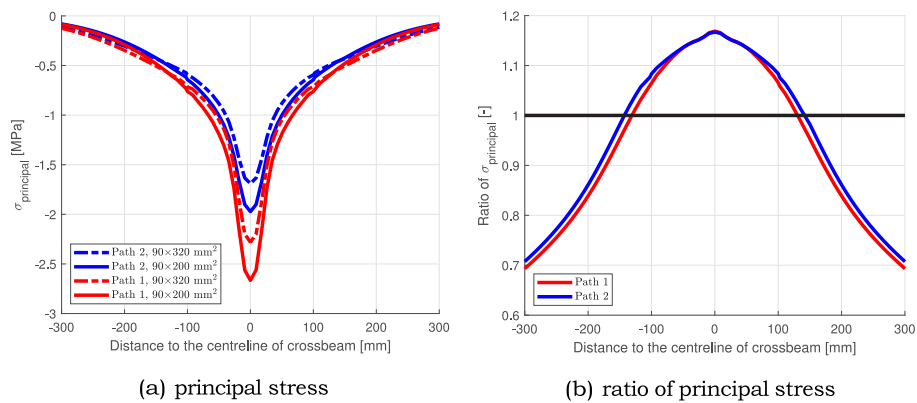


Fig. 23. Principal stress distribution along the selected paths in Fig. 22.

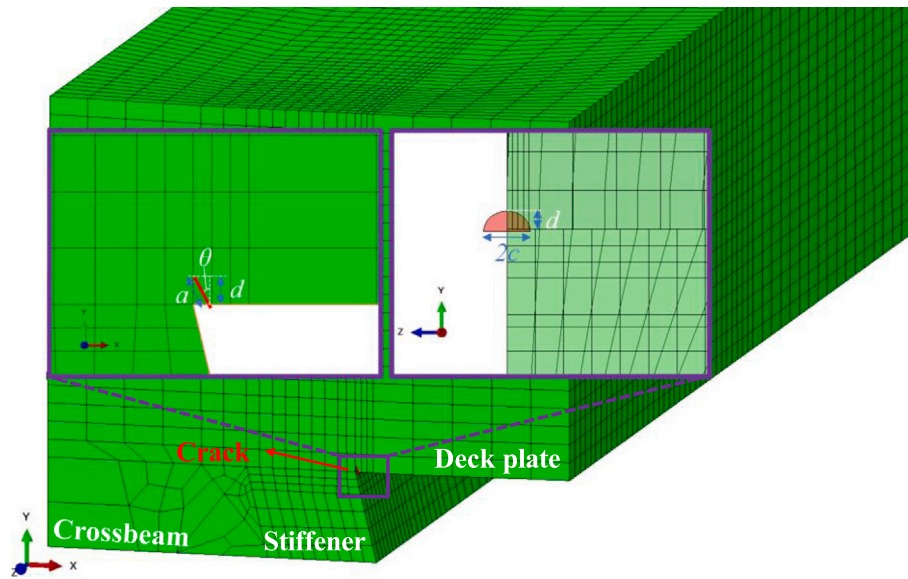


Fig. 24. Illustration of the XFEM model for C1c type crack.

propagates further in the length direction. Crack arrest in the depth direction occurs after the crack depth reaches approximately 75% of the deck plate thickness with 16 mm and 20 mm thick deck plates, while the crack propagates further in the length direction (defined as failure type 3), see the lengths at the top ($2c_{top}$) and bottom ($2c_{bottom}$) of the deck plate in Fig. 25. In the simulations, the crack inclines towards the horizontal direction. The results are in qualitative agreement with the experimental observation in [2,9,12,33,36].

5. Conclusions

Experimental investigation and FE analyses are employed for studying the fatigue behaviour of the stiffener-to-deck plate weld in OBDs, with a crack in the deck plate initiating from the weld root at the crossbeam intersection (detail C1c according to [24]). Different from the previous publications, the deck plate is relatively thick, thereby representing a new generation of OBDs. One full-scale specimen with a 20 mm thick deck plate is loaded, resulting in sixteen C1c type cracks. The stress and strain distribution, crack propagation, fatigue resistance using the hot spot stress, and lack of weld penetration are studied. Additionally, fatigue crack propagation paths are calculated using the XFEM for different plate thicknesses. The main conclusions are:

1. The maximum stress in the stiffener-to-deck plate welded connection at crossbeam intersection occurs at the weld root. Fatigue cracks initiating from the weld root at the crossbeam and propagating into the deck plate are observed in the experimental study. With a 20 mm thick deck plate, the crack arrest occurs at an approximate depth of 14 to 15 mm. This is approximately 75% of the deck plate thickness.
2. Using the authors' own results and data in the literature, the recommended characteristic fatigue resistances using hot spot stress are:
 - **112 MPa** for early cracking according to the measurement of strain gauges.
 - **170 MPa** for the earliest visible crack detection criterion from the top of the deck with a deck plate thickness of 10 mm to 12 mm.
3. A lack of penetration of up to 1.5 mm (75% penetration ratio) does not significantly influence the ENS.

4. The crack propagation path calculated from the XFEM using linear elastic fracture mechanics is similar to the experimental results with 10 mm, 12 mm, 16 mm, and 20 mm thick deck plates tested by the authors or in the literature. After reaching 75% of the total deck plate thickness, the crack stops propagating in the thickness direction for the deck plates thicker than 12 mm. Through thickness crack occurs in 10 mm thick deck plate. For 12 mm thick plate, the final crack is very close to the top surface and can break through at high load levels. Moreover, root cracks in the weld throat and stiffener are observed at the junction with crossbeam in line with experimental observation.

CRediT authorship contribution statement

Weijian Wu: Writing – original draft, Visualization, Validation, Software, Methodology, Investigation, Formal analysis, Data curation, Conceptualization. **Milan Veljkovic:** Writing – review & editing, Supervision, Methodology. **Henk Kolstein:** Supervision, Data curation, Funding acquisition. **Richard Pijpers:** Validation, Data curation. **Johan Maljaars:** Writing – review & editing, Validation, Supervision.

Declaration of competing interest

The authors declare that they have no known competing financial interests or personal relationships that could have appeared to influence the work reported in this paper.

Data availability

Data will be made available on request.

Acknowledgements

The experimental study is sponsored by the Dutch bridge asset owner Rijkswaterstaat (RWS). The authors acknowledge Frank van Dooren from RWS for the discussions in the project meetings. Akram Elkazaz is acknowledged for his contribution to the XFEM simulation. The first author would like to thank China Scholarship Council, China for the study funding.

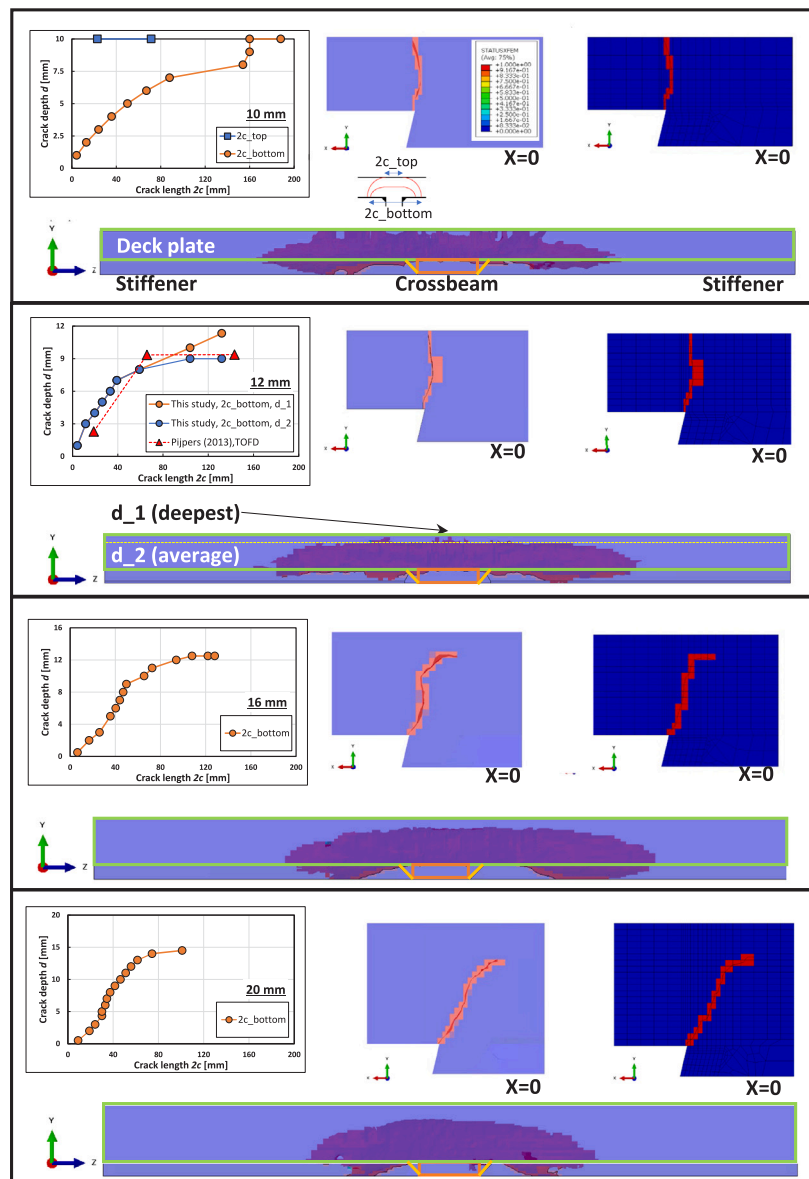


Fig. 25. Crack shapes from the XFEM for 10 mm, 12 mm, 16 mm, and 20 mm thick deck plates (the load patches $270 \times 320 \text{ mm}^2$ for 12 mm thick deck plate, and $180 \times 320 \text{ mm}^2$ for other thicknesses) [33].

References

- [1] Kolstein MH. Fatigue classification of welded joints in orthotropic steel bridge decks (doctoral thesis), Delft, The Netherlands: Delft University of Technology; 2007.
- [2] De Jong FBP. Renovation techniques for fatigue cracked orthotropic steel bridge decks (doctoral thesis), Delft, The Netherlands: Delft University of Technology; 2006.
- [3] Zhang Q, Cui C, Bu Y, Li Q. Experimental study on fatigue features of orthotropic bridge deck through full-scale segment models. *Tumu Gongcheng Xuebao/China Civ Eng J* 2015;48(4).
- [4] Chen W-F, Duan L. Orthotropic deck bridges. In: Chen W-F, Duan L, editors. *Bridge engineering handbook*. CRC Press; 2000.
- [5] Wolchuk R. Lessons from weld cracks in orthotropic decks on three European bridges. *Journal of Structural Engineering* 1990;116:75–84.
- [6] Beales C, Cunningham JR. Strengthening and refurbishment of Severn crossing. Part 4: TRRL research on Severn crossing. *Proc ICE - Struct Build* 1992;94(1):37–49.
- [7] Hobbacher AF. In: Mayer C, editor. *Recommendations for Fatigue Design of Welded Joints and Components*. International Publishing; 2016.
- [8] Maljaars J, van Dooren F, Kolstein H. Fatigue assessment for deck plates in orthotropic bridge decks. *Steel Constr* 2012;5(2):93–100.
- [9] Hayashi N, Kudo Y, Okumura M, Uchida D, Mori T. Influence of load range on fatigue crack propagation behavior in orthotropic steel deck. In: 4th orthotropic bridge conference proceedings. Tech. rep., Tianjin.
- [10] Mehue P. Cracks in steel orthotropic decks. *Bridge Manage* 1990;633–42.
- [11] Tsakopoulos PA, Fisher JW. Fatigue resistance investigation for the orthotropic deck on the Bronx-Whitestone Bridge. *arc*, no. 02, 2002.
- [12] Konda N, Nishio M, Ichimiya M, Kasugai T, Kiyokawa S. Development of fatigue test method and improvement of fatigue life by new functional steel plates for welding of trough rib and deck plate of orthotropic decks. *Int J Steel Struct* 2013;13(1):191–7.
- [13] Maljaars J, Bonet E, Pijpers RJ. Fatigue resistance of the deck plate in steel orthotropic deck structures. *Eng Fract Mech* 2018;201:214–28.
- [14] Wu W, Kolstein H, Veljkovic M. Stress intensity factors of the rib-to-deck welded joint at the crossbeam conjunction in OSDs. *Proc Struct Integr* 2018;13:2017–23.
- [15] EN 1993-1-9. Eurocode 3: Design of steel structures - Part 1-9: Fatigue. Brussels, Belgium: European Committee for Standardization; 2005.
- [16] pr EN1993-1-9. Eurocode 3: Design of steel structures – Part 1-9: Fatigue. doc n3751 (enquiry draft). Brussels, Belgium: European Committee for Standardization; 2023.
- [17] DNVGL-RP-C203. Recommended practice - fatigue design of offshore steel structures. Oslo: DNV (DNVGL); 2016.
- [18] pr EN1993-1-14. Eurocode 3: Design of steel structures — Part 1-14: Design assisted by finite element analysis (final draft). Brussels, Belgium: European Committee for Standardization; 2021.

- [19] AASHTO. AASHTO LRFD Bridge Design Specifications. 6th ed.. American Association of State Highway and Transportation Officials; 2012.
- [20] Connor R, Fisher J, Gatti W, Gopalaratnam V, Kozy B, Leshki B, McQuaid DL, Medlock R, Mertz D, Murphy T, Paterson D, Sorensen O, Yadlosky J. Manual for Design, Construction, and Maintenance of Orthotropic Steel Deck Bridges 2012.
- [21] Maljaars J, van Dooren F, Kolstein H. Fatigue assessment for deck plates in orthotropic bridge decks. *Steel Constr* 2012;5(2):93–100.
- [22] Kozy BM, Connor RJ, Paterson D, Mertz DR. Proposed revisions to AASHTO-LRFD bridge design specifications for orthotropic steel deck bridges. *J Bridge Eng* 2011;16(6):759–67.
- [23] Tsakopoulos PA, Fisher JW. Fatigue resistance investigation for the orthotropic deck on the Bronx-Whitestone Bridge. ATLSS report No. 02-05, 117 ATLSS Drive Bethlehem, PA, the United States; 2002.
- [24] prTS 1993-1-901. Fatigue design of orthotropic bridge decks with the hot spot stress method (final draft). Brussels, Belgium: European Committee for Standardization; 2023.
- [25] EN 10025-2. Hot rolled products of structural steels. Part 2: Technical delivery conditions for non-alloy structural steels. Brussels, Belgium: European Committee for Standardization; 2004.
- [26] Lillemäe I, Remes H, Liinalampi S, Itävu A. Influence of weld quality on the fatigue strength of thin normal and high strength steel butt joints. *Welding in the World* 2016;60(4):731–40.
- [27] Jonsson B, Dobmann G, Hobbacher AF, Kassner M, Marquis G. IIW guidelines on weld quality in relationship to fatigue strength, In: IIW collection, 1st ed.. Vol. 1, Cham: Springer International Publishing; 2016.
- [28] Maljaars J, Pijpers R, Wu W, Kolstein H. Fatigue resistance of rib to deck, crossbeam to deck and deck to deck welds in orthotropic decks using structural stress. *Int J Fatigue* 2023;175:107742.
- [29] ISO 5817. Welding-Fusion-welded joints in steel, nickel, titanium and their alloys (beam welding excluded) - Quality levels for imperfections. 2014.
- [30] Wu W, Kolstein H, Veljkovic M. Fatigue crack propagation analysis of rib-to-deck welded joint in OSDs using linear elastic fracture mechanics. In: IABSE symposium, nantes 2018: tomorrow's megastructures. 2018.
- [31] De Bree D. TOFD inspection report on selected areas of the Classification Trough cover plate C33B78 (in Dutch). Tech. rep., Infra Inspectie B.V.; 2016.
- [32] Charlesworth J. Engineering applications of ultrasonic time-of-flight diffraction. 2nd ed.. Research Studies Pre; 2002.
- [33] Pijpers R. Structural health monitoring for fatigue life prediction of orthotropic bridge decks. In: 3rd orthotropic bridge conference. Sacramento CA., USA; 2013.
- [34] De Jong FBP, Kolstein MH. Strengthening a bridge deck with high performance concrete. In: 2004 orthotropic bridge conference. 2004.
- [35] NEN EN 1993-1-9/NA. Dutch national annex to Eurocode 3: Design of steel structures – Part 2: Steel bridges. Nederlands Normalisatie Instituut; 2012.
- [36] Dung CV, Sasaki E, Tajima K, Suzuki T. Investigations on the effect of weld penetration on fatigue strength of rib-to-deck welded joints in orthotropic steel decks. *Int J Steel Struct* 2015;15(2):299–310.
- [37] EN 1990. Eurocode - Basis of structural design. Brussels, Belgium: European Committee for Standardization; 2002.
- [38] Bartsch H, Drebenstedt K, Seyfried B, Feldmann M, Kuhlmann U, Ummenhofer T. Analysis of fatigue test data to reassess EN 1993-1-9 detail categories. *Steel Constr* 2020;13(4):280–93.
- [39] Simulia. Abaqus user's manual version 2019. 2019.
- [40] Radaj D, Sonsino CM, Fricke W. Fatigue Assessment of Welded Joints by Local Approaches: 2nd ed.. Elsevier; 2006.
- [41] Yazid A, Abdelkader N, Abdelmadjid H. A state-of-the-art review of the X-FEM for computational fracture mechanics. *Appl Math Model* 2009;33(12):4269–82.